Analysis of radar-rainfall error characteristics and implications for streamflow simulation uncertainty

EMAD HABIB, ANANDA V. ADUVALA & EHAB A. MESELHE

Department of Civil Engineering and Center for Louisiana Water Studies, University of Louisiana at Lafayette, PO Box 42291, Lafayette, Louisiana 70504-2291, USA

habib@louisiana.edu

Abstract Due to the inherent indirect nature of radar-rainfall measurements, hydrologists have been interested in understanding the characteristics of radar-rainfall estimation errors and how they propagate through hydrological simulations. This study implements an observational-based empirical approach to analyse different characteristics of the total radar-rainfall estimation error such as overall and conditional bias, random error, and spatio-temporal dependence. The implications of the radar error characteristics for streamflow simulations and the estimation of their uncertainty are examined using a physically-based distributed rainfall-runoff model. An empirical error model is used to generate several realizations of probable surface rainfall fields that reflect the identified characteristics of the radar error. These realizations are used to generate ensemble of streamflow predictions. The main conclusions are that: (a) radar errors have complex spatio-temporal characteristics that exhibit significant sampling and natural variations; (b) adjustment of overall and conditional radar biases results in the most significant improvements in runoff predictions; (c) radar random errors have non-negligible correlations both in time and space; (d) the simulated runoff hydrographs are sensitive to the assumed degree of correlation in the radar errors fields. This study is an initial step toward developing more rigorous approaches for accounting for the effects of radar error on hydrological predictions.

Key words: radar-rainfall estimation; sensitivity; error propagation; streamflow; modelling

Title in French: **Analyse des caractéristiques d'erreurs entre données radar et pluviométriques ainsi que les répercussions sur l'incertitude des simulations d'écoulement**

Résumé: Du fait de la nature indirecte inhérente aux observations pluviométriques par radar, les hydrologues s'efforcent de comprendre les caractéristiques des erreurs des estimations pluviométriques basées sur les observations radar, et la manière dont ces erreurs se propagent dans les simulations hydrologiques. La présente étude applique une approche empirique fondée sur les observations pour analyser différentes caractéristiques de l'erreur totale, telles que erreur systématique et aléatoire, et leur dépendance spatio-temporelle. Les implications des caractéristiques des erreurs d'observations radar sur les simulations d'écoulement et sur l'estimation de leurs incertitudes sont examinées à l'aide d'un modèle hydrologique distribué simulant l'écoulement. Un modèle empirique de génération d'erreurs est utilisé pour produire plusieurs champs de précipitation probables qui reflètent les caractéristiques identifiées pour les erreurs du radar. Ces réalisations sont utilisées pour générer un ensemble de prédictions d'écoulement. Les principales conclusions tirées de cette application sont que (a) les erreurs des observations radar ont des caractéristiques spatio-temporelles complexes qui présentent une répartition significative et des variations naturelles; (b) l'ajustement des erreurs systématiques générales et propres au radar permet d'obtenir les améliorations les plus significatives dans la prédiction des écoulements; (c) les erreurs aléatoires des observations radar sont correlées de manière non négligeable dans le temps et l'espace; (d) les hydrographes simulés sont sensibles au degré de correlation des champs d'erreur de radar. Cette étude représente un premier pas vers le développement d'une approche plus rigoureuse pour prendre en compte les effets des erreurs d'observations radar sur les prédictions hydrologiques.

Mots-clés: estimations d'erreurs de radars pluviométriques, sensibilité, propagation d'erreur, modélisation d'écoulement

INTRODUCTION

Recent technological and scientific advances in weather radars present unprecedented opportunities for providing accurate and timely rainfall information. The extensive spatial coverage and relatively high temporal and spatial resolutions of weather radar systems are valuable

for hydrological prediction and forecasting applications. In particular, recent developments in physically-based distributed hydrological models (Singh & Woolhiser, 2002) sparked increasing interest in the use of distributed radar-rainfall information (Tachikawa *et al*., 2003). However, it is recognized that radar-rainfall estimates are associated with significant uncertainties that arise from various factors such as: hardware calibration, significant variations and non-uniqueness in the relationship between radar-measured reflectivity (Z) and rainfall rate (R), range-related effects, beam overshooting and partial beam filling, anomalous propagation of the radar beam, and the non-uniformity in vertical profiles of reflectivity (VPR) (see detailed discussions in Wilson & Brandes, 1979; Austin, 1987; Hunter, 1996; Rico-Ramirez *et al*., 2007). Quantification of such uncertainties and how they affect hydrological predictions has proved to be a challenging task (Krajewski & Smith, 2002). The focus of the present study is to gain a better understanding of the radar error characteristics and the subsequent sensitivity of rainfall-runoff simulations to different aspects of these characteristics. Proper identification of radar-induced uncertainties in runoff modelling is relevant for streamflow ensemble forecasting studies. For example, if streamflow observations fall outside the forecast ensemble, then further revisions are needed in the formulation of the model and its structure (Hossain *et al*., 2004; Gourleya & Vieux, 2006). Uncertainty bounds that are unrealistically too wide or too narrow can lead to false conclusions regarding the adequacy of the utilized data and the adopted hydrological model and its parameters.

Since the advent of the weather radar systems, numerous studies have been conducted to examine the utility of radar-rainfall information in runoff modelling. Bedient *et al*. (2000) indicated that radar data resulted in flood predictions as accurate as raingauge data. Sun *et al*. (2000) indicated that, without the use of optimal estimation methods, radar data could result in errors greater than those associated with gauge observations. Preliminary analysis by Johnson *et al*. (1999) showed comparable performance of radar and gauge with some instances of erroneous results in the case of radar-based simulation. Different results were reported in Obled *et al*. (1994) which showed that using distributed rainfall information did not lead to improved hydrograph simulations. Pessoa *et al*. (1993), Vieux & Bedient (1998) and Morin *et al*. (2005) tested the sensitivity of runoff simulations to Z-R relationships and suggested that appropriate identification of the relationship parameters is necessary to obtain accurate runoff forecasts. Winchell *et al*. (1998) found higher sensitivity of runoff prediction to the established Z-R relationship in the case of infiltration-excess runoff generation mechanism than in the case of saturation-excess mechanism. Neary *et al*. (2004) emphasized the need for correcting long-term biases of radar-rainfall estimates before they can be used in operational hydrological studies. Borga (2002) analysed the effects of variability in radar vertical profile of reflectivity (VPR) on streamflow simulations. The interaction of VPR errors with model parametric uncertainty was investigated recently by Hossain *et al*. (2004). Radar beam geometric and sampling-related effects were analysed by Sharif *et al*. (2002), which showed that range effects and storm-watershed orientation-related errors get amplified through runoff predictions.

Common to the above mentioned studies is their focus on individual sources of the radar error. However, in practical applications, separating and estimating the different sources of radar errors is not possible. An alternative approach to this problem focuses on the estimation of the total radar uncertainty (Ciach et al., 2007; German *et al*., 2006) through comparison of radar estimates versus independent reference surface rainfall information. Earlier studies such as Krajewski & Georgakakos (1985) and Krajewski *et al*. (1993) have proposed time-space stochastic modelling of the total radar error. However, due to lack of accurate surface rainfall measurements, recent applications of this approach in hydrological modelling studies were based on simplified assumptions regarding the distribution of the radar error and its spatial and temporal dependence properties (e.g. Carpenter & Georgakakos 2004; Butts *et al*., 2004). In fact, in most error-modelling studies, spatial and temporal correlations of radar error fields were neglected. Carpenter & Georgakakos (2004) recognized this problem and indicated the need for more realistic representation of the radar error and its propagation into hydrological models. The need to account for error dependency was recently investigated (Nijssen & Lettenmaier, 2004; Hossain & Anagnostou,

2006) for satellite precipitation estimates, which have error properties that are quite different from those of the radar estimates. Jordan *et al*. (2003) developed and calibrated a random cascade model of radar errors that accounts for error correlations. Their results indicated non-negligible levels of error correlations especially in space. However, their model dealt with correlations of reflectivity errors that are caused mainly by variations in VPR.

In a recent operationally-oriented effort, Ciach et al., (2007) formulated a comprehensive approach to empirically model the combined sources of the radar error based on analysis of joint samples of radar and ground reference rainfall data. In the present study, we follow this approach to examine the marginal and joint statistical properties of the radar error and investigate their relative significance for estimating uncertainties in runoff predictions. Instead of focusing on a certain source of the error, we deal with the combined radar error, which can be estimated by analysis of radar-rainfall data against accurate reference surface rainfall information. We use radar-rainfall estimates from the Stage-III operational precipitation products that are based on the national WSR-88D NEXRAD radar system in the United States. Reference surface rainfall data over the scale of the radar pixels are constructed from high-resolution raingauge measurements collected within a mid-size humid watershed. Analysis of the joint radar and reference samples enables us to examine two main aspects of the radar error: systematic (bias) and random. We first estimate the bias component of the radar error and examine its variability in time (storm to storm) and space (pixel to pixel). Besides the overall bias, we also assess the conditional dependence of the radar bias on rainfall intensities (Ciach *et al*., 2000). The implications of bias characteristics for the accuracy of runoff predictions are addressed by analysing 12 significant rainfall-runoff events using a physically-based distributed hydrological model. We then construct and fit an empirical model for the random error component in which the radar error is a function of the rainfall intensity. Besides the marginal properties of the random error component, we also investigate its spatial and temporal dependence properties. A simple ensemble generator that takes into account the identified radar error statistical characteristics is implemented to generate realizations of spatial fields of probable rainfall estimates over the study watershed. Finally, we use the generated rainfall fields to study the sensitivity of ensemble flow simulations produced by the distributed model to the prescribed characteristics of radar errors especially their spatial dependence. We close with discussions on the implications of the results for future modelling studies on the propagation of radar error through hydrological predictions.

STUDY SITE AND EXPERIMENTAL DATA

The Goodwin Creek (GC) experimental watershed located at the north part of Mississippi (Alonso & Binger, 2000) was selected for this study (Fig. 1). The watershed has a fairly steep topography with drainage area of 21.4 km^2. The terrain elevation in the watershed with reference to mean sea level ranges from 71 m near the outlet to 128 m at the catchment divide with an average channel slope of 0.004. It has a humid climate (hot in summer and warm in winter), an average annual

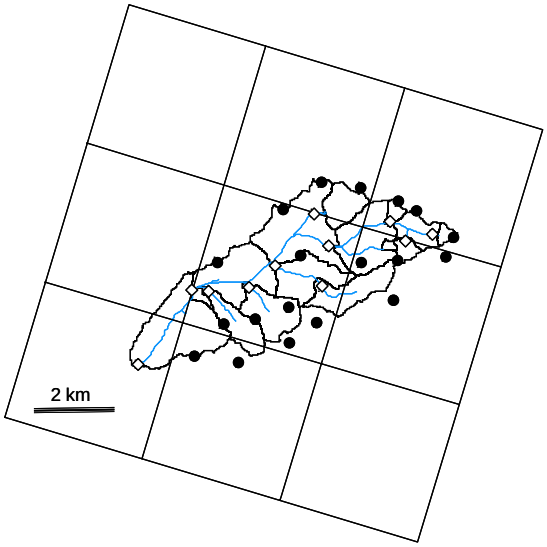

Fig. 1 The Goodwin Creek study watershed in north central Mississippi showing the locations of the raingauges (circles and diamonds) and the discharge gauges (diamonds). The rectangular grid represents the 4×4 km^2 HRAP grid of the Stage III radar data.

Table 1 Summary of rainfall-runoff simulation events.

Storm	Storm date	Storm duration (h)	Total rainfall depth (mm)	Total runoff depth (mm)	Maximum 1-hour rainfall intensity (mm/h)	Maximum runoff peak (m^3/s)
1	18 January 2002	19	41.9	26.1	9.4	27.0
2	22 January 2002	27	36.0	23.2	12.7	25.4
3	24 January 2002	26	81.5	70.6	27.3	40.6
4	5 February 2002	39	24.6	10.1	5.1	5.8
5	19 February 2002	8	44.2	25.2	19.1	36.5
6	15 March 2002	11	15.7	8.8	15.9	5.8
7	16 March 2002	44	33.3	21.2	9.0	13.8
8	20 March 2002	24	38.1	27.2	8.4	17.7
9	26 March 2002	9	20.3	6.3	11.7	7.0
10	29 March 2002	42	71.4	47.9	10.7	26.6
11	8 April 2002	20	24.1	4.9	5.6	6.3
12	2 May 2002	61	130.6	74.3	21.8	57.5

temperature of about 65°F, an average annual rainfall of about 1440.2 mm (56.7 inches), and an average annual runoff of 144.8 mm (5.7 inches). The land use in the watershed can be described as follows: pasture (44%), forest (27%) cultivated land (14%) and gullied land (15%). The soil can be classified into two main types: silt loam (80%) and clay loam (20%). The dominant runoff generation process in the GC watershed is infiltration-excess mechanism.

Long-term hydrometeorological data have been continuously collected in the watershed since 1981 (Fig. 1) by the National Sediment Laboratory of the US Department of Agriculture in Oxford, Mississippi. A dense network of over 30 raingauges distributed within the watershed is used to measure precipitation. After careful quality control checks, data from only 30 gauges will be used in the current analysis. Continuous streamflow records are collected at the watershed outlet in addition to other several interior locations. Meteorological data necessary for runoff modelling (e.g. solar radiation, wind speed, relative humidity) are available from a weather station located approximately 130 km north of the GC watershed. In this study, a total of 12 significant rainfall-runoff events during the wet non-growing season are considered for analysis of the radar rainfall hydrological simulations (Table 1). These events were grouped into two continuous simulation periods (January–February and March–May 2002), to be modelled in a continuous

mode. Durations of the events ranged from few hours to few days. Event-total rainfall volumes were in the range of 15 to 130 mm. Maximum hourly rainfall intensities exceeded 20 mm h^{-1} during two storms with most storms in the range of 5–20 mm h^{-1}. For most of the selected storms, runoff-rainfall ratios were high (up to 86%), and discharge peaks reached as high as 57.5 m^3 s^{-1} (equivalent to a unit peak of 2.69 m^3 s^{-1} km^{-2}).

The Goodwin Creek watershed is under coverage from four Weather Surveillance Radar – 1988 Doppler (WSR-88D) NEXRAD radars. The closest of these radar sites is located near Memphis, Tennessee, approximately 120 km to the north of the catchment. In this study, the Stage III operational precipitation products of the NEXRAD system are used. These products are available over the area of the Goodwin Creek watershed from the National Weather Service (NWS) Lower Mississippi River Forecast Center (LMRFC). Stage III products are hourly accumulations of precipitation over a grid of approximately 4x4 km^2 that is usually referred to as HRAP grid (Hydrologic Rainfall Analysis Project, Reed & Maidment, 1999). A full description of Stage III algorithm is available in numerous publications (e.g. Fulton *et al*., 1998) and only a brief description is provided herein. Development of the Stage III data is a three-step process that starts from the raw radar reflectivity field (Z). In Stage I, a power law Z–R relationship is applied to estimate fields of precipitation rates, R, that are then integrated over time to produce hourly accumulations. The result of the Stage I process is radar-only products known as Digital Precipitation Products (DPA) (Smith *et al*., 1996). In Stage II, gauge observations are used to construct the mean field bias for the radar estimates, which is then used to produce bias-adjusted radar precipitation estimates over the HRAP cells. In addition, a gauge-only precipitation field is produced and optimally merged with the bias-adjusted radar field to produce the Stage II products. The final step involves "mosaicking" of Stage II products from multiple radars to produce a single Stage III product over the LMRFC region. An assessment of the quality and accuracy of Stage III rainfall estimates is provided in several studies (e.g. Young *et al*. 2000; Jayakrishnan *et al*. 2004), which indicate that despite bias adjustment, biases as well as significant random errors are still present in these estimates.

RAINFALL-RUNOFF MODEL FOR THE STUDY WATERSHED

In the current study, the Gridded Surface Subsurface Hydrologic Analysis (GSSHA) modelling system is used to develop a rainfall-runoff model for the GC watershed. GSSHA is a fully distributed-parameter process-based hydrological model (Downer & Ogden, 2002, 2004). It uses finite difference and finite volume methods to simulate different hydrological processes such as rainfall distribution and interception, overland water retention, infiltration, evapotranspiration, two-dimensional overland flow, and one-dimensional (1-D) channel routing. The GSSHA system also provides a detailed modelling of the soil moisture profile in the unsaturated zone using different methods such as Green and Ampt and Richards' equation.

The model setup adopted in this study is similar to that used by Senarath *et al*. (2000), who developed a model for the same watershed using the hydrological model CASC2D (an earlier formulation of GSSHA). The following modelling options are used in our study: two-dimensional diffusive wave approximation of the de Saint Venant equations for overland flow, 1-D explicit diffusive wave method for channel flow, Penman-Monteith equation for evapotranspiration calculations, and the Green and Ampt infiltration with redistribution method (Ogden & Saghafian, 1997) for flow simulation in the unsaturated zone. This infiltration method includes soil moisture accounting and allows for continuous long-term simulations that contain sequence of dry and wet periods. The soil moisture accounting scheme simulates the soil moisture redistribution along the soil profile during a runoff event, as well as the change in soil moisture due to evapotranspiration between rainfall events. In the current study, rainfall events were grouped into two long periods (January–February and March–May 2002; Table 1) and each one of them was modelled in a continuous mode.

The watershed topographic and hydrological properties were represented using a square

Cartesian grid with a resolution of 125 × 125 m^2. According to Senarath *et al*. (2000), this resolution provides an adequate spatial representation of the soil and land-use properties in the watershed. Topographic information for the watershed was obtained from the US Geological Survey 30-m digital elevation maps. Channel cross-sectional dimensions were compiled from historical surveys. Overland hydraulic properties (e.g. roughness parameters) were assigned at each grid pixel based on land use information. Similarly, soil hydraulic parameters necessary for the Green and Ampt method (e.g. saturated hydraulic conductivity, soil suction head, effective porosity), and evapotranspiration parameters (e.g. vegetation transmission coefficients and root depth) were assigned based on spatial variations in the combined classifications of the soil type and land use maps. Initial values of these parameters were selected based on literature sources and (a) (b)
ues reported in Senarath *et al*. (2000) and Dow Ogden (2004). The selected values will be adjusted through a model-calibration procedure.

Prior to using the GSSHA model to assess the effects of radar-rainfall errors, the model needs to undergo a careful calibration process so that it can provide accurate representation of the rainfall-runoff transformation in the watershed. In this study we performed calibration and validation analyses where one set of continuous rainfall-runoff periods (April–May 1982 and February–March 1987) was used to calibrate the model while other periods (shown in Table 1) were reserved for model validation. The calibration was designed to minimize the overall differences between observed and simulated runoff hydrographs. The main model parameters adjusted during the calibration procedure included soil infiltration parameters and overland and

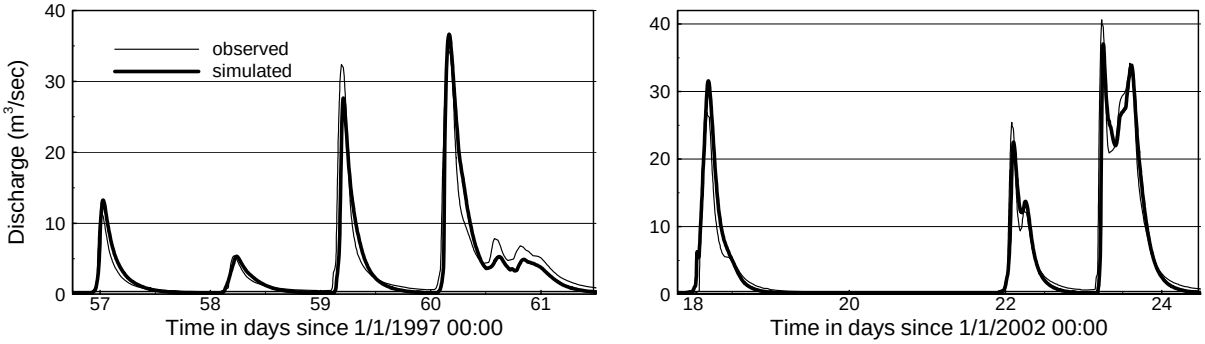

Fig. 2 (a) GSSHA calibration and (b) validation results. Simulations are driven by distributed rainfall measurements from the 30 raingauges in the GC watershed.

channel roughness coefficients. However, the simulated runoff peaks and volumes were most sensitive to changes in the soil saturated hydraulic conductivity and to a lesser degree to the overland and channel roughness coefficients. Figure 2 shows typical examples of the model calibration and validation results for some of the modelled simulation periods. The results indicate that the model is well calibrated and will likely provide physically reasonable representation of the important runoff processes within the GC watershed. This was confirmed by the final values of the calibrated model parameters which we found to be within physically reasonable bounds. To provide a quantitative assessment of the model uncertainty (due to parameter estimation, model structure, etc.), we computed model errors in simulating timing and magnitude of runoff peaks during the calibration and validation periods. Out of 16 significant peaks, eight were predicted with errors less than 10%, three peaks had errors between 10 and 15%, two had errors between 20 and 25%, and only two had errors that reached up to 30%. Model errors in predicting time-to-peak were mostly less than 20–30 min.

ANALYSIS OF SYSTEMATIC COMPONENT OF RADAR ERROR

Overall bias

The most basic characteristic of the radar error is overall bias (B), which represents systematic average deviations of radar estimates (R_r) with respect to the corresponding surface rainfall over the radar pixel size (R_s):

$$B = \frac{E[R_s]}{E[R_r]} \tag{1}$$

where E[•] denotes the expectation operator.

Quantifying and correcting for the bias will guarantee that the radar estimates agree on average with the rainfall quantities that actually reach the surface. This property is most desirable for hydrological applications where long-term systematic deviations in rainfall input can be detrimental to model-calibration efforts. To examine bias variability over space and from storm to storm, we estimate the bias factors for each radar pixel over the watershed (Fig. 1) and for each storm separately (Table 1) using the following multiplicative form:

$$B_{i,j} = \frac{\sum_{l=1}^{l=nh}\left[\frac{1}{np}\sum_{k=1}^{k=np} G_{i,j,k,l}\right]}{\sum_{l=1}^{l=nh} R_{i,j,l}} \tag{2}$$

where $G_{i,j,k,l}$ and $R_{i,j,l}$ represent the lth gauge and radar hourly rainfall rates, respectively, for storm i and pixel j, nh is the number of hours in each storm, and np is the number of raingauges in pixel j. In this formula, surface pixel-average rainfall rate is obtained by averaging observations from several raingauges located within the pixel. This provides highly accurate estimates of storm totals especially for the central radar pixel, which is densely covered with 13 raingauges. For other pixels, a fewer number of gauges, or even one gauge, can still provide acceptable estimates of storm total rainfall volume. This was verified when we compared storm rainfall total volumes from individual gauges within the central pixel. This comparison showed minor differences (mostly less than 5%) amongst the individual gauges. We should note that raingauge measurements are known to be subject to their own local uncertainties such as wind-undercatch, wetting and evaporation losses, and random errors due to the gauge sampling mechanism (Sevruk & Lapin, 1993; Habib *et al*., 2001; Upton & Rahimi, 2003). Except for the wind-induced losses (which are significant only under strong wind conditions), most of these errors become almost negligible when aggregating rainfall data to hourly or storm-total temporal scales (Habib *et al*., 2001; Ciach, 2003) as done in equation (2). For smaller time scales (e.g. a few minutes), gauge measurement errors can be significant and should be taken into account in analysing radar uncertainties (Habib *et al*., 2004).

An assessment of the overall bias of the Stage III products over the GC watershed is shown in Fig. 3. Although originally adjusted with raingauge measurements, the Stage III data still contain considerable bias values that range from about 0.4 to 1.6. As expected, bias varies significantly from one storm to another. Spatial variations in bias estimates across the different pixels are also evident for most of the analysed storms, but to a lesser degree.

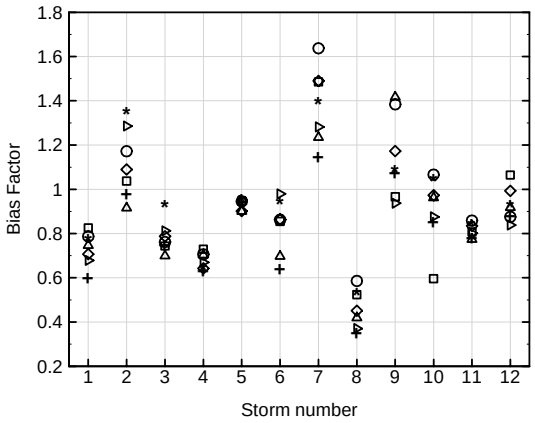

Fig. 3 Storm overall bias associated with the Stage III radar data. Different symbols for each storm correspond to different pixels over the watershed.

Conditional bias

Besides the overall bias, Ciach *et al*. (2000) showed that radar bias can also depend on the magnitude of the estimated rainfall itself. This property, which is referred to as conditional bias, CB, describes how a specific radar estimate differs on average from the corresponding surface rainfall rate. The CB statistic can be expressed in a multiplicative conditional form as follows:

$$\mathrm{CB}(r_r) = \frac{E\{R_s \mid R_r = r_r\}}{r_r} \tag{3}$$

where r_r denotes a certain value of the radar-rainfall estimate R_r. Similar to Ciach et al., (2007), we estimated the conditional bias using a conditional moving average:

$$\mathrm{CB}(a < R_r \le b) = \frac{\overline{R_s} \mid (a < R_r \le b)}{\overline{R_r} \mid (a < R_r \le b)} \tag{4}$$

where the over-bar symbol denotes arithmetic averaging, and a and b represent the bounds of the moving averaging window. This window had a varying size that was selected in such a way to ensure reasonable sample sizes necessary for averaging. Similar to the overall bias, the surface rainfall, R_s, was estimated from simple averaging of all gauges inside each radar pixel. Given the storm-to-storm variability in the estimated overall bias factors, we estimated CB for each storm separately. However, due to the reduction of sample sizes caused by conditioning, the conditional sub-samples of (R_s, R_r) were constructed by combining data from all pixels in each storm so that reasonable sample sizes were still available for averaging.

The estimated CB values are shown in Table 2 for three examples of the analysed storms. As expected, CB depends on the radar estimate; however, the behaviour of such dependence was different from one storm to another. For most storms (e.g. Storm 1) CB decreased with R_r, which indicates (as also reported in previous studies) that radar tends to overestimate high rainfall rates and underestimate low rainfall rates. Other storms showed either an opposite behaviour (e.g. Storm 9), or a rather uniform conditional bias (e.g. Storm 12) that does not depend on rainfall intensity. While the estimated overall and conditional bias values might be subject to sampling effects, the results indicate the complex behaviour of the radar error, even when dealing with its basic characteristics such as the bias.

Table 2 Analysis of conditional Stage III biases (estimated using equation (4)) for three selected example storms.

Storm	Radar rain rate (mm/h)	Conditional bias, CB
1	0–0.5	3.6
	0.5–1.3	1.15
	1.3–2.5	0.63
	2.5–5.1	0.59
	5.1–8.9	0.72
	>8. 9	0.74
9	0–0.7	0.24
	0.7–3.2	0.96
	3.2–4.6	1.42
	4.6–6.4	1.14
	>6.4	1.06
12	0–0.8	0.82
	0.8–2.3	0.8
	2.3–3.8	0.9
	3.8–6.1	1.06
	6.1–11.7	0.92
	>11.7	0.9

Effect of radar bias on runoff prediction

The above analysis indicated that the radar bias has complex characteristics such as spatial and storm-to-storm variability and conditional dependence on the radar estimates. To investigate the relative contribution and impact of these characteristics on rainfall-runoff simulations, we applied different bias-adjustment corrections to the Stage III radar data. Several well-documented bias-adjustment correction schemes have been developed and tested for real-time applications (e.g. Anagnostou & Krajewski, 1998; Seo & Breidenbach, 2002). However, since the focus of this study is not on real-time use of radar data, we will apply three simple correction methods in which different aspects of the radar bias can be examined. The first method corrects the overall bias for each storm and ignores bias spatial variations. The second method corrects the bias at each pixel and for each storm. The third method estimates the bias with conditioning on the radar estimate. In this method bias spatial variations could not be considered to avoid further reductions in the sample sizes. The three methods account for storm-to-storm bias variability. For brevity, we will term the three methods as: spatially-uniform unconditional; spatially-dependent unconditional; and spatially-uniform conditional.

Comparison of radar and surface rainfall Prior to assessing the bias effect on runoff prediction, we first examine how the bias-corrected radar estimates compare with the corresponding surface rainfall rates. Each bias-correction method was applied to the Stage III data by simply multiplying the radar estimate by the estimated bias factor. Each corrected radar data was then compared against the average raingauge observations inside each pixel. The comparison is quantified for each storm in terms of two statistical measures: the ratio of radar to surface rainfall storm totals, and the root mean squares of differences (RMSD) between radar and surface hourly rainfall rates. An example of the comparison results is shown in Fig. 4 for the central pixel. For reference, the comparisons also include the raw Stage III data without any bias adjustment. Consider first the plot showing the storm bias ratios (Fig. 4(a)). As expected, all three methods have resulted in a significant adjustment in the radar storm accumulations. Obviously, a perfect agreement in the storm-total rainfall volume is obtained in the central pixel when the Stage III data are adjusted using spatially-dependent (i.e. pixel-specific) bias factors. The bias correction not only resulted in adjusting storm rainfall totals, but also improved the overall agreement between

hourly radar and surface estimates. Compared to the unadjusted Stage III data, considerable reductions in the RMSD are obtained (Fig. 4(b)) after applying the bias-correction methods. The most basic bias adjustment (spatially-uniform, unconditional) reduced the radar RMSD in most of the storms (seven out of 12). Using conditional-bias adjustment resulted in further improvements in the RMSD in some storms (e.g. 2, 5 and 6). This indicates that accounting for bias dependence on the radar estimates will ensure the overall unbiasedness of the radar products and will also help improve their accuracy in terms of random deviations from the reference surface rainfall. Similar observations were also made by Vignal & Krajewski (2001), who reported a decrease in radar random errors as a result of correcting radar biases that were caused by variations in the radar vertical profile of reflectivity. As argued by Krajewski & Smith (2002), bias effects are caused by different and competing sources, which, when combined together, appear random. As shown in the current study, this problem can be addressed in an off-line analysis by using conditional bias corrections rather than a simple overall bias removal.

Analysis of simulated hydrographs The calibrated GSSHA model was used to simulate runoff using radar data during the selected 12 rainfall-runoff storms in 2002 (Table 1). To examine the effects of different bias characteristics, model simulations were driven with several rainfall inputs: original Stage III data and data adjusted using each of the three methods described above.

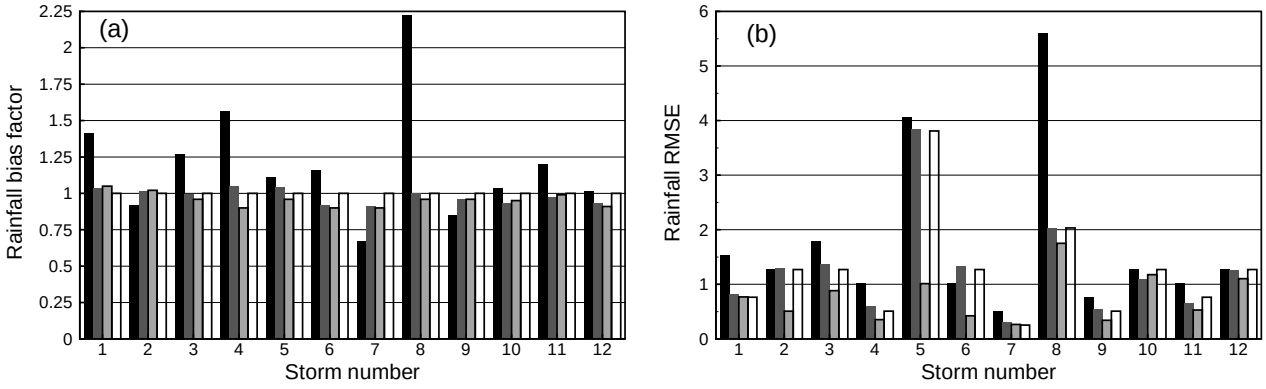

Fig. 4 Rainfall bias (a) and RMSE (b) for different bias correction methods. For each storm, column bars ordered from left to right represent the following bias adjustment methods: no adjustment, spatially-uniform unconditional, spatially-uniform conditional, and spatially-dependent unconditional (see text for more explanation).

To isolate the effects of the radar bias, we compared the radar-driven simulated hydrographs against "reference" runoff simulations driven by pixel-averaged raingauge measurements. By doing so, we focus on radar-related runoff prediction errors without being dominated or affected by other modelling and parameter estimation uncertainties. This also unifies the spatial scales of the reference and radar input data. The adequacy of these reference simulations was confirmed (not shown here) by checking them against runoff measurements and against simulations driven by fully distributed (i.e. not pixel-averaged) rainfall measurements from the 30 raingauges in the watershed (same as those used in the calibration tests of Fig. 2).

Differences between radar-driven and reference hydrographs are evaluated both visually (see two example storms in Fig. 5) and statistically using the following measures:

$$\text{Runoff bias for each storm: } B = \frac{\sum_{i=1}^{i=n} Q_i^{\text{ref}}}{\sum_{i=1}^{i=n} Q_i^{\text{rad}}} \tag{5}$$

Runoff RMSD for each storm: $$\mathrm{RMSD} = \sqrt{\frac{1}{n}\sum_{i=1}^{i=n}(Q_i^{\mathrm{ref}} - Q_i^{\mathrm{rad}})^2} \quad (6)$$

Runoff peak error for each peak in each storm: $$P_e = \frac{P^{\mathrm{rad}} - P^{\mathrm{ref}}}{P^{\mathrm{ref}}} \quad (7)$$

where n is the number of discharge values within each storm (one value every five minutes), Q represents runoff discharge, P represents runoff peak, and the two superscripts, "ref" and "rad", denote simulations using reference rainfall input (raingauges averaged over each pixel) and simulations using a certain radar data (unadjusted or adjusted using each of the three bias correction methods), respectively.

A summary of these statistical measures is presented in Fig. 6 for the 12 simulated storms. Figures 5 and 6 show several features that are worth noting. Consider first the hydrographs obtained using the original unadjusted Stage III radar data. Despite significant deviations, these hydrographs show relatively similar overall patterns to the corresponding reference hydrographs. This indicates the ability of the Stage III radar estimates to capture the overall spatial and temporal structure of the storms, at least qualitatively. However, significant bias levels are clearly seen both in the plotted hydrographs (Fig. 5) and in the calculated runoff bias factors for each storm

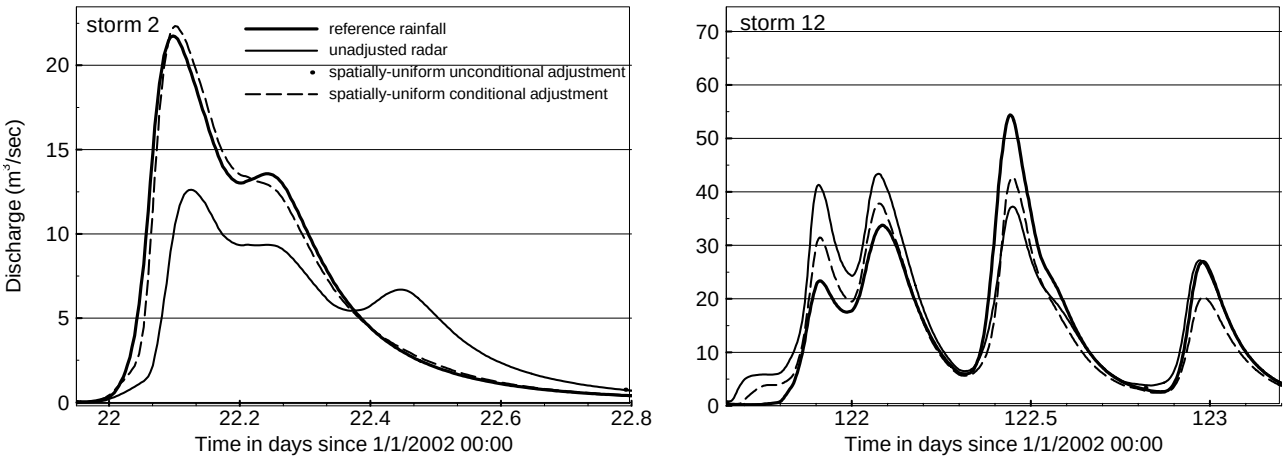

Fig. 5 Simulated runoff hydrographs using different bias adjustment methods for two example storms. Results obtained with spatially-dependent unconditional bias adjustment were similar to those of the spatially-uniform unconditional adjustment, and are not shown for figure clarity.

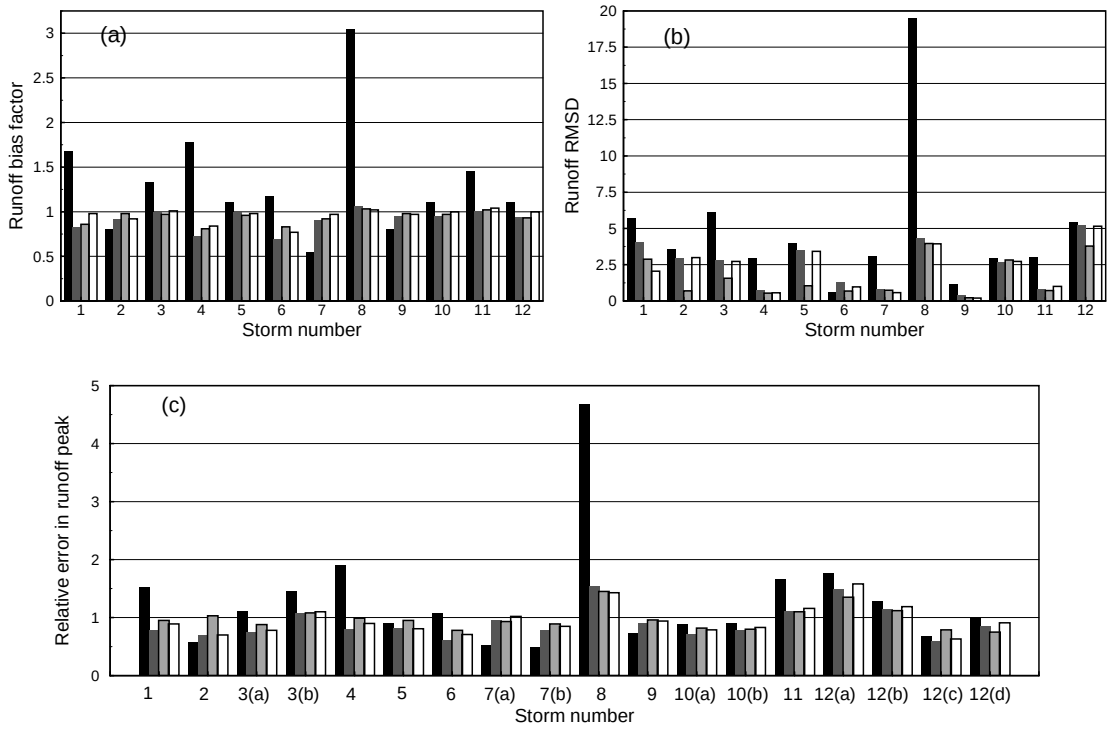

Fig. 6 Statistical assessment of effect of radar bias on runoff prediction: (a) runoff bias, (b) runoff RMSE, and (c) runoff peak error. Column bars are the same as those in Fig. 4.

(Fig. 6(a)). By plotting rainfall *vs* runoff bias ratios (not shown here), it was also interesting to notice that biases in radar-rainfall estimates got enhanced as they propagated through the simulated runoff hydrographs. The overall and conditional radar biases presented earlier (Table 2 and Fig. 4) have also resulted in relatively poor runoff prediction performance as reflected in the large runoff RMSD values (Fig. 6(b)) and the high relative peak errors (Fig. 6(c)).

Correction of overall biases has resulted in a significant improvement in the radar-based hydrographs. Runoff bias and RMSD and relative peak errors decreased significantly for all of the storms. A remarkable improvement is evident (Fig. 6) for storms 3, 4 and 8 during which the original Stage III estimates suffered from apparently high bias levels (Fig. 4(a)). While most of the simulated hydrographs gained an immediate benefit after removing the overall bias, further improvements were obtained as a result of accounting for bias dependence on the estimated radar rain rates. In storms 2, 3, 4, 5, 6 and 12, the runoff RMSD attained the lowest values when conditional bias removal was applied (Fig. 6(b)). The rest of the storms showed almost equivalent performance for any of the applied bias correction methods. Note that accounting for spatial bias variations improved runoff predictions in only one storm (Storm 1). This is mainly due to the relatively small area of the watershed and its coverage by few radar pixels only. It is important to note that while the removal of radar biases resulted in improving the runoff prediction accuracy, residual differences are still apparent in some of the simulated hydrographs and their performance statistics compared to the corresponding results of the reference rainfall input. This is probably due to the random radar error component that remains in the radar rainfall input. The characteristics of this random component and its effect on the runoff prediction are analysed next.

ANALYSIS OF RANDOM COMPONENT OF RADAR ERROR

As shown above, conditional bias removal results in the most significant improvement in the radar-rainfall estimates and their runoff predictions. Therefore, for the remainder of this study, we will work with the Stage III data after removing its bias using the spatially-uniform conditional

adjustment. Having adjusted for the radar bias, the radar error can now be considered purely random, which can be expressed using the following form:

$$\varepsilon = \frac{R_s}{R_r} \tag{8}$$

In the following, we attempt to identify the distribution of the random component by analysing joint hourly radar and surface pixel-average rainfall samples. We focus on estimating marginal properties of the error distribution (e.g. mean and variance), as well as its statistical dependence structure (e.g. spatial and temporal correlations).

Modelling of the radar random error

An essential prerequisite for estimating the random component of the radar error (equation 8) and its distribution is an accurate approximation of the true hourly surface rainfall over the radar pixel domain, R_s, which can be obtained using raingauge measurements inside the radar pixel. As we discussed earlier, most of the local random gauge errors get averaged out at hourly accumulation scales, however, the inability of individual near-point gauge measurements to represent areal-average rainfall over the size of a radar pixel (4×4 km^2) remains of concern (Wood *et al.*, 2000). To overcome this problem, it has been customary to approximate R_s by averaging observations from multiple raingauges located within the pixel. The accuracy of such approximations will depend on the number and configuration of gauges within the pixel, and on the degree of sub-pixel rainfall natural spatial variability. Therefore, we first examined the adequacy of the number of gauges and their configuration in each pixel in the watershed. We did this by calculating the error variances of the pixel gauge-average approximations using a well-established statistical measure, the Variance Reduction Factor (VRF) (Bras & Rodriguez-Iturbe, 1993). The VRF provides a relative measure of the error variance of areal-rainfall approximations obtained using a certain number and configuration of gauges within the area of interest. Calculations of the VRF require specification of the rainfall spatial correlation function. We used a common isotropic exponential model of the spatial correlations as a function of distance and fitted it to the inter-gauge hourly correlations calculated from the GC raingauge network. We computed VRF for each pixel in the watershed. For comparison, we also computed the VRF for a hypothetical case of a single gauge located in the center of the radar pixel, which was found to be equal to 0.09. As expected, the best (i.e. lowest) VRF (0.006) was obtained in the central pixel which contains the highest number of gauges. The highest VRF values (0.1 and 0.11) were obtained for the two lower left pixels. Compared to the hypothetical case of a single gauge, the upper right pixel and the middle right pixel showed significantly improved VRF (0.024 and 0.028). According to the VRF calculations, it is clear that the dense gauge arrangement within the central pixel can provide relatively accurate approximation, R_s. However, to increase the size of the joint sample (R_r,R_s), and to allow for examining the spatial dependence of the radar error field, we decided to additionally include two more pixels (upper and middle right pixels) since their number and configuration of gauges has resulted in relatively low VRF values.

Using hourly gauge averages in each of the three selected radar pixels, we computed the radar hourly random error using equation (8) and plotted it against the corresponding radar estimates (Fig. 7(a)). We also computed the empirical cumulative probability distribution (CDF) of the error and compared it to the cases of normal and lognormal distributions, which are commonly utilized in rainfall modelling studies (Fig. 7(b)). Clearly, the lognormal distribution provides a better fit to the random component of the radar error. This distribution is completely defined by the first two moments of either the logarithmically-transformed variable, $\ln(\varepsilon)$, or the original variable ε. The results shown in Fig. 7(a)) indicate that, due to the applied conditional bias removal, the mean of ε, μ_ε, does not depend on the radar estimate and is almost equal to one. Unlike the mean, it is clear that the standard deviation of ε, σ_ε, depends on R_r. Similar to the case of the conditional bias (equation (4)), we used the following moving-average estimator with an adaptable window size to

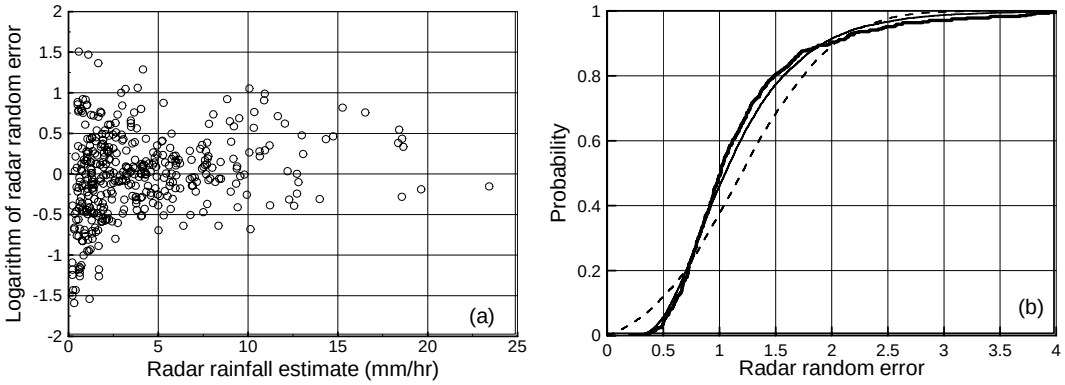

Fig. 7 (a) Scatter plot of the radar random error, (equation (9)), as a function of the corresponding radar-rainfall estimate R_r. (b) Empirical cumulative distribution function (cdf) of the error (thick continuous line) compared to the corresponding theoretical cdf of normal (dashed line) and lognormal (thin continuous line) distributions.

describe the dependence of σ_ε on R_r:

$$\sigma_\varepsilon^2(a < R_r \le b) = \overline{(\varepsilon - \mu_\varepsilon)^2} \mid (a < R_r \le b) \tag{9}$$

As seen in Fig. 7(a), σ_ε attains high levels at small R_r values, but decreases gradually with the increase of R_r. The conditional dependence of σ_ε on R_r can be conveniently approximated and modelled using the following formula:

$$\sigma_{\varepsilon|R_r}^2 = \alpha(R_r)^{-\beta} \tag{10}$$

where α and β are empirical fitting coefficients.

Spatial and temporal dependence of radar error

We now examine the joint properties of the error distribution to assess its spatial and temporal dependence. We do so by estimating the temporal and spatial auto-correlation of ε. Using the marginal samples of ε estimated for each of the three selected pixels, we calculated the auto correlation of ε at different time lags (Fig. 8). We also calculated spatial correlations between errors of the three pairs of pixels combined together (Fig. 9), which represents the 4-km lag correlation of ε. Correlations at larger spatial lags cannot be analysed herein due to the limited number of pixels that provide accurate approximation of the true pixel-average surface rainfall. Spatial and temporal auto-correlations were estimated for each storm separately, and then for all storms combined. Results for storms with sample sizes that are too small to be adequate for estimating correlation coefficients are not displayed. The main observation in the plotted results is that both the temporal and spatial correlations of ε are non-negligible. However, the temporal auto-correlation is rather low (mostly less than 0.4) at small lags (1 or 2 h) and becomes close to zero for larger time lags. Negative correlations are also observed in the temporal correlation coefficients. The spatial correlation exhibits stronger levels for most of the analysed storms. For some storms, the spatial correlation was high (0.8 and above). Notice the significant variations in the estimated correlations between different storms (in case of temporal and spatial correlations) and between different pixels (in case of temporal correlation). However, some of these variations might be attributed to the limited sample sizes, which affect the estimation of correlation coefficients especially for skewed distributions (Kessler & Neas, 1994; Habib & Krajewski, 2001). When combining all storms, the sampling effect becomes less important and the temporal correlations show more stable, but still low, values (solid lines in Fig. 8). Similarly, the spatial correlations between pairs of pixels, but without accounting for intra-storm variability (solid line in Fig. 9), maintains rather medium correlation values (~0.5).

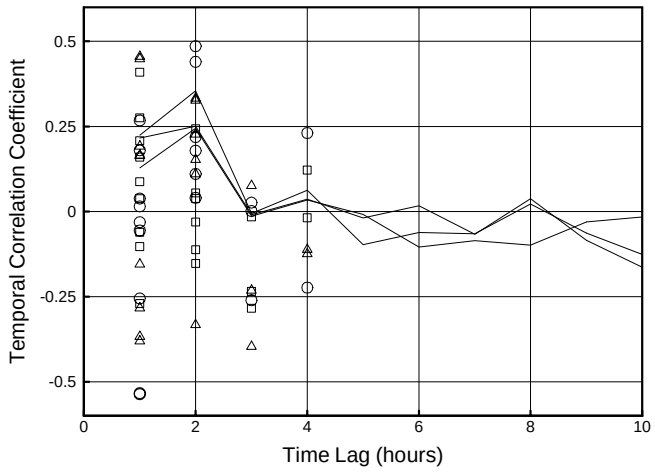

Fig. 8 Empirical temporal auto-correlations of the random component of the radar error. The three symbol types represent correlations calculated at the three selected radar pixels. For each lag, points plotted with the same symbol represent correlations of different storms. The three lines are correlations calculated after combining all storms. Beyond a 4-hour lag, the sample size becomes too small to calculate correlation coefficients for individual storms.

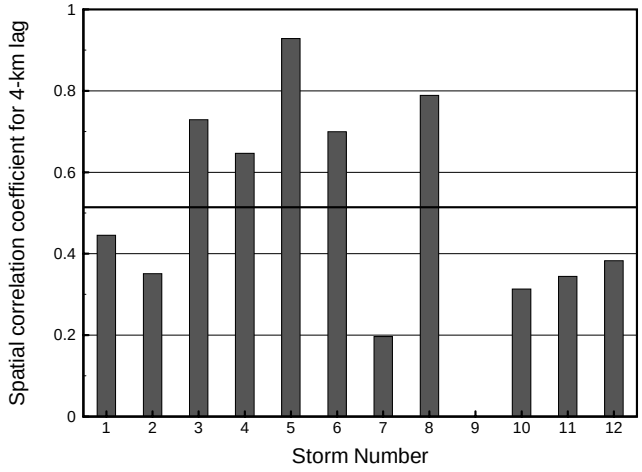

Fig. 9 Empirical spatial auto-correlations of the random component of the radar error at one spatial lag (4 km) calculated for each storm separately. Correlations are calculated between errors in the three pairs of radar pixels combined together. The solid line is the correlation value calculated after combining all storms.

Sensitivity of runoff hydrographs

The fitted lognormal distribution of the radar error, identified by its constant mean and R_r-dependent standard deviation (equation (10)), provides a suitable tool to model the multiplicative radar random error. It also allows for generating multiple realizations of probable surface rainfall fields that reflect the uncertainty associated with actual radar-rainfall estimates. However, in generating such realizations, one has to account for the empirically observed dependence structure of the error. Since temporal correlations were found to be rather low, we focus our analysis on accounting for the spatial dependence only. The generated lognormally-distributed error fields should have a mean of one and a standard deviation that depends on the observed radar estimate, and should be correlated in space (over one 4-km lag only). We generated such correlated random fields using a statistical procedure (The Math Works, Natick, MA) that is based on the Cholesky decomposition method. The generated fields of ε are then substituted in

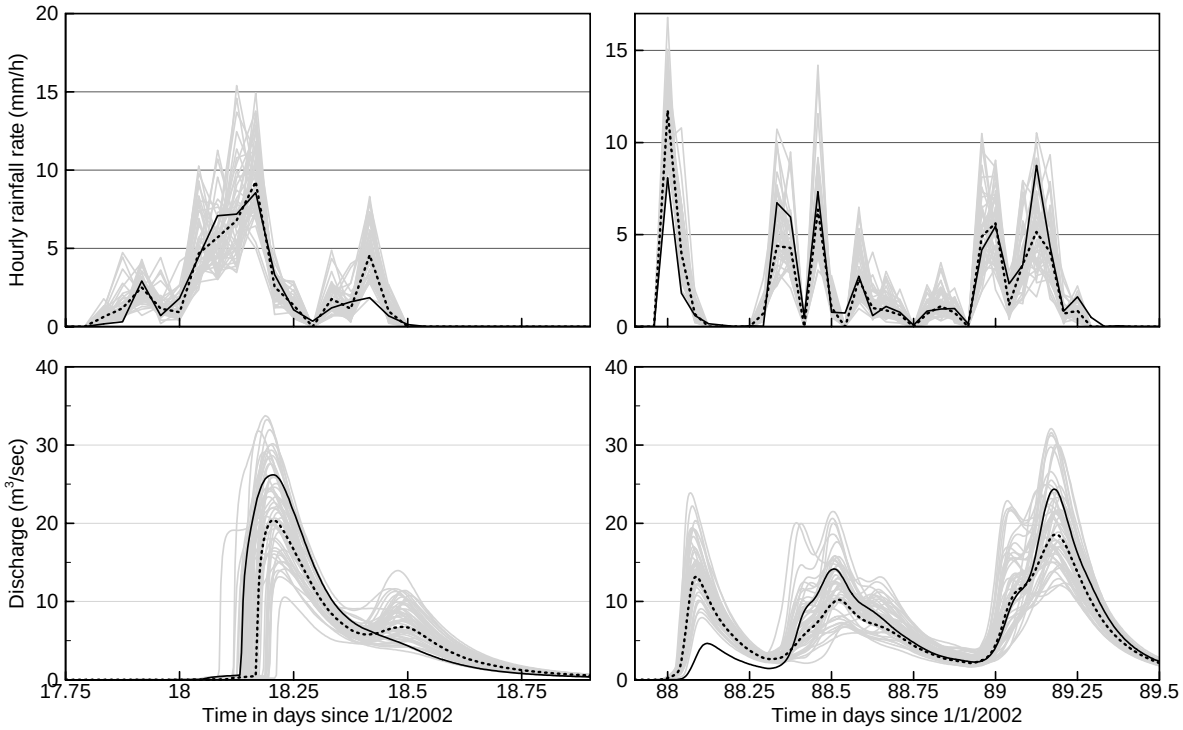

Fig. 10 Upper panels show 50 realizations of probable surface rainfall time series (grey lines) generated for two example storms using a value of 0.6 for the 4-km lag spatial correlation of the radar error. Also shown are the reference surface rainfall data (continuous dark line) and the bias-adjusted Stage III radar data (dotted line). Lower panels show the corresponding simulated runoff hydrographs.

equation (8) to provide the corresponding realizations of probable surface rainfall fields that take into account the identified characteristics of the radar error. An example of such analysis is shown in Fig. 10 for two selected storms. The corresponding time series of the actual radar data (bias-corrected Stage III estimates) and the reference surface rainfall (average of gauges in each pixels), are shown in the same figure for the central pixel. Similar rainfall realizations are generated for the other analysed storms. Each realization is then used as input to the GSSHA hydrological model resulting in an ensemble of predicted runoff hydrographs (Fig. 10). Examining the plotted rainfall ensembles indicates that, as was incorporated in the empirical error model, the spread of the generated realizations depends on the magnitude of the radar Stage III value (R_r). For most hours within the storm, the reference rainfall input falls within the generated rainfall ensemble and the predicted ensemble runoff hydrographs also enclosed the reference hydrograph that was based on accurate surface rainfall information. This indicates the ability of the fitted-error model to characterize radar uncertainties and to explain the observed deviations of the radar-based runoff predictions from the reference hydrographs.

In the example shown above, a value of 0.6 was used as the spatial auto-correlation to generate the radar error fields. However, recognizing the difficulties inherent in estimating the "true" spatial dependence structure of the radar error (Fig. 9), and to examine the sensitivity of the propagation of radar uncertainties to different levels of error correlations, we repeated the above analysis using two more correlation values: 0 and 0.95. These values represent two scenarios where radar errors are assumed to be either fully uncorrelated or strongly correlated in space. The hydrograph ensembles obtained with the three examined spatial auto-correlation levels are summarized in terms of their 2.5 and 97.5 percentiles calculated at each hour within the storm (see Fig. 11 for few example storms). The difference between the two percentile lines represents the

95% uncertainty range in the predicted hydrographs due to the effect of radar random errors. Several remarks can be made about the plotted runoff uncertainty bounds. Consider first the

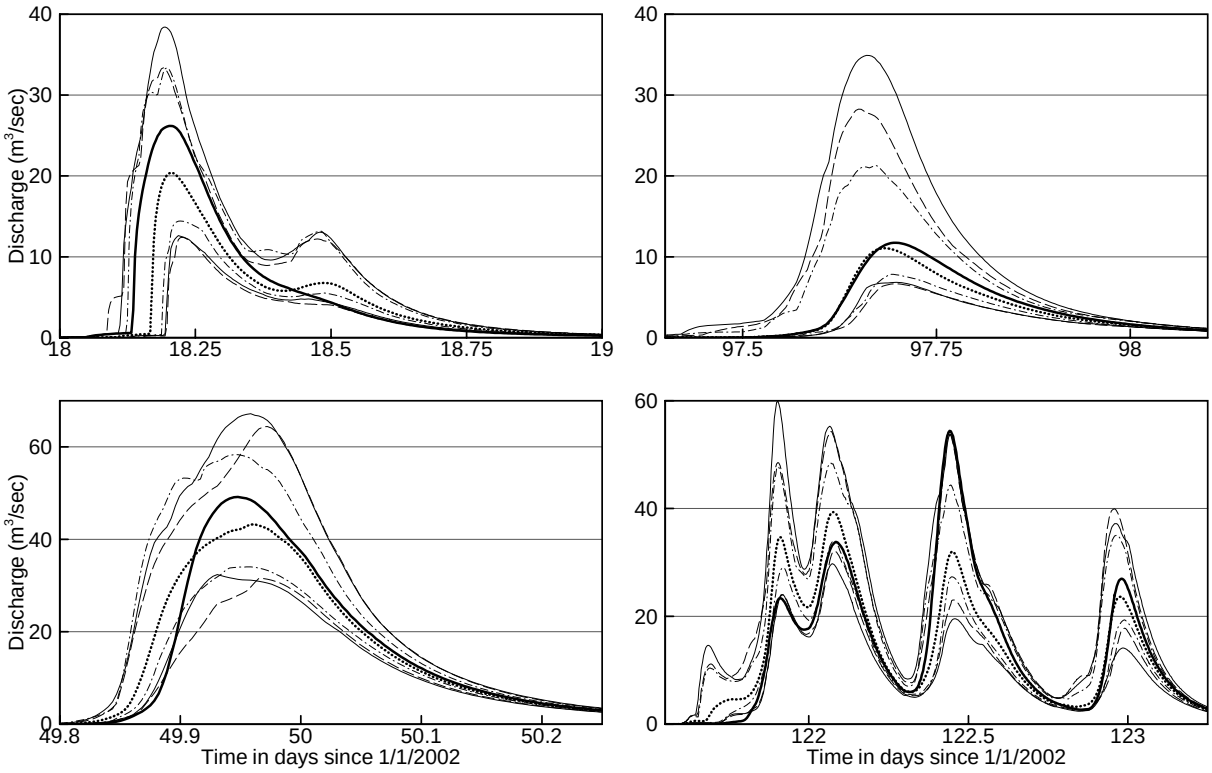

Fig. 11 97.5% and 2.5% percentiles of the hydrograph ensembles using three different spatial auto-correlation values: 0 (dash-dotted line), 0.6 (dashed line), and 0.95 (thin continuous line). The thick continuous and thick dotted lines represent runoff obtained using the reference surface rainfall input and the bias-adjusted Stage III data, respectively.

bounds obtained with a certain error correlation value. The estimated bounds show clear variations during the storm duration. In general, they are wider during the rising limbs of the hydrographs than during the falling limbs. For storms with single-peak hydrographs, runoff uncertainty bounds have a well-defined and systematic behaviour. They increase gradually along the rising part of the hydrograph until they reach a maximum value just before the hydrograph peaking time, and then start to decrease gradually during the receding part of the hydrograph. For storms with more complex patterns (i.e. with multiple bursts of rainfall and runoff peaks), the patterns and relative magnitudes of the uncertainty bounds become more complex too. The increased runoff uncertainty during the rising parts of the hydrographs reflects the enhanced sensitivity of the early-generated runoff to rainfall variability, and more importantly to uncertainties in the rainfall estimates and the introduced degree of spatial error dependence.

The calculated runoff percentiles are sensitive to the assumed spatial auto-correlation level of the radar error especially for the upper percentile (97.5%). Using a high error correlation value (0.95) resulted in much wider runoff uncertainty bounds than those obtained with low (0) or medium (0.6) correlations. Again, the runoff uncertainty bounds are more sensitive to error correlations during the rising limbs of the hydrographs, but much less sensitive during falling limbs where the percentile lines of the three spatial correlation levels are almost indistinguishable. It is also worth noting that the degree of sensitivity to the assumed level of error correlation is not always the same as it varies from one storm to another.

Finally, for most storms, runoff hydrographs obtained using the reference rainfall data lie within the 95% uncertainty range of the hydrograph ensembles for the three assumed values of the error spatial correlation. However, for some hours within the storms, the 95% uncertainty ranges enveloped the simulated reference hydrographs only when a certain level of error correlation is used. This indicates that the assumed correlation value affect the estimated width of the estimated runoff uncertainty bounds and whether they can explain the differences between radar-driven runoff predictions and those obtained using the reference rainfall input.

SUMMARY AND CONCLUDING REMARKS

In this paper we analysed errors of radar-rainfall estimates focusing on its two main components: systematic (bias) and random. We studied the characteristics of each error component and their implications for the accuracy of runoff predictions in a humid mid-size watershed. The results indicated that, despite being subject to operational bias-removal procedures, the analysed Stage III radar data still suffered from systematic deviations from the reference surface rainfall. Further adjustments of such deviations seem to provide the most significant improvement in runoff predictions in terms of runoff volumes and peaks. The overall radar bias showed significant variations both spatially (pixel-to-pixel) and temporally (storm-to-storm). However, given the limited size of the watershed, accounting for temporal (storm-to-storm) variability proved more important for runoff prediction purposes. Besides the overall bias, further improvements were obtained after correcting for the radar bias in a conditional way. Conditional accounting for the bias dependence on the radar estimates improved the overall unbiasedness of the radar estimates and reduced their random deviations from the reference surface rainfall. Subsequent improvements were evident in the hydrographs of several of the simulated storms. We note that the bias removal implemented here was at the scale of storm total accumulations. This “off-line” mode was adopted to understand the properties of the systematic component of the radar error (i.e. overall and conditional biases) and their relative contribution to the uncertainty in runoff predictions. Further analysis can be conducted to examine the effect of other elaborate real-time bias adjustment schemes on the accuracy of rainfall-runoff predictions.

Radar random errors were estimated empirically based on comparison to raingauge measurements in three pixels covering the watershed. A main limitation on the implementation of this approach is the requirement to have access to a dense raingauge network that can be used to approximate “true” surface rainfall. The analysis indicated that simple error models (e.g. normal distribution with constant variance) are not adequate to capture the statistical characteristics of the random component. Instead, an empirical model based on the lognormal distribution was fitted to approximate the multiplicative radar random error component. The fitted lognormal distribution has a standard deviation that decreases with the increase of the radar rainfall estimate. We also examined the temporal and spatial dependence of the radar error by calculating its auto-correlation coefficients at various temporal lags (one hour and above) and one spatial separating distance (4 km). One-hour lag temporal correlations were found to be non-negligible, but rather low. The 4-km lag spatial auto-correlation coefficients attained more significant levels for many of the analysed storms.

The effect of the error random component and its spatial correlation on the simulated runoff hydrographs was examined. Runoff uncertainty bounds caused by the modelled radar uncertainties were estimated and found to be quite wide especially during the rising periods of the hydrographs. These bounds were also sensitive to the assumed level of spatial correlation of the error. The sensitivity was most significant during the rising parts of the hydrographs and much less significant during the receding periods. In some of the simulated events, reference runoff simulations were enclosed within the runoff uncertainty bounds only when a certain error correlation level was used to model the radar error spatial dependence. This finding indicates the need for further research aiming towards better characterization of the dependence structure of radar errors and accounting for their effects in radar-based runoff modelling studies.

The analyses performed in this study were based on radar products developed by a specific algorithm (Stage III) and at certain scales (hourly and 4×4 km^2). Similar analyses can be performed on other radar products focusing on their particular error characteristics. However, we expect that the general findings regarding the properties of the radar error and the observed sensitivity of hydrological predictions to be applicable to other radar datasets. Another issue is whether the current results can be generalized to watersheds characterized with runoff generation mechanisms and climatic conditions that are different from the Goodwin Creek study watershed. Further analysis is needed to address this question given the fact that rainfall uncertainties interact with the characteristics of the watershed as they propagate through the various modelled hydrological processes. We also note that this study was based on analysis of a relatively small-size watershed (21.4 km^2) with low to moderate rainfall hourly intensities (less than 30 mm/h). The specific results on radar error characteristics and the mechanism by which they propagate through runoff simulations are expected to vary across different watershed scales (i.e. from small to large-size watersheds) and rainfall characteristics (i.e. from low to high intensities). Extending this analysis to include more rainfall-runoff storms and other watershed sizes and locations is therefore recommended.

We finally note that it was not the intent of this study to provide a comprehensive answer to the challenging question on how radar rainfall errors impact hydrological modelling predictions (see further discussions in Krajewski & Smith, 2002; Carpenter & Georgakakos, 2004). Instead, the present work attempted to provide insight into the complex spatio-temporal characteristics of the radar error at hydrologically-relevant scales and how they impact our interpretation of uncertainties in flow simulations. The reported results suggest that using over-simplified approaches for modelling the radar errors, or ignoring their dependency structure, could lead to unrealistic representation of hydrological model uncertainties. This is further complicated by the evident variability in the estimated radar error statistical characteristics (systematic and random errors and spatio-temporal dependency), either at the storm scale or for the whole sample. The source of such variability is possibly a combination of actual variations that reflect the complexity of these characteristics, and variations caused by sampling effects. This highlights the need for special observational setups that can provide accurate reference rainfall information at high resolutions. Such information is necessary for better characterization of the radar error characteristics especially at small temporal and spatial scales, which are becoming increasingly desired in recent hydrological modelling applications.

The complexity evident in the estimated runoff uncertainty bounds calls for more in-depth investigations on the propagation of radar errors into runoff prediction models. Currently, most studies have focused on analysis of the end predictable variable of these models (i.e. streamflow). We believe that tracking the errors through the different hydrological processes simulated by the model (e.g. infiltration, soil moisture variations, evapotranspiration losses, and surface and channel flow) might give better insight into the error propagation and how it interacts with the different modelling components. Current efforts are underway by the authors to implement this process-based error propagation analysis.

REFERENCES

Alonso, C. V. & Binger, R. L. (2000) Goodwin Creek experimental watershed: A unique field laboratory. *J. Hydraul. Engng ASCE* **126**, 174–177.

Anagnostou, E. N. & Krajewski, W. F. (1998) Calibration of the NEXRAD precipitation processing subsystem. *Weather Forecast.* **13**, 396–406.

Austin, P. M. (1987) Relation between measured radar reflectivity and surface rainfall. *Mon. Weather Rev.* **115**, 1053–1070.

Bedient, P. B., Hoblit, B. C., Gladwell, D. C. & Vieux, B. E. (2000) NEXRAD Radar for flood prediction in Houston. *J. Hydrol. Engng ASCE* **5**(3), 269–277.

Borga, M. (2002) Accuracy of radar rainfall estimates for stream flow simulation. *J. Hydrol.* **267**, 26–39.

Bras, R. L. & Rodriguez-Iturbe, I. (1993) *Random Functions and Hydrology*. Dover, New York, USA.

Butts, M. B., Payne, J. T., Kristensen, M. & Madsen, H. (2004) An evaluation of the impact of model structure on hydrological modeling uncertainty for streamflow simulation. *J. Hydrol.* **298**, 242–266.

Carpenter, T. M. & Georgakakos, K. P. (2004) Impacts of parametric and radar rainfall uncertainty on the ensemble streamflow

simulations of a distributed hydrological model. *J. Hydrol.* **298**, 202–221

Ciach, G. J. (2003) Local random errors in tipping-bucket rain gauge measurements. *J. Atmos. Oceanic Technol.* **20**, 752–759.

Ciach, G.J., Krajewski, W.F. & Villarini, G. (2007) Product-error-driven uncertainty model for probabilistic quantitative precipitation estimation with NEXRAD data, J. Hydrometeorology, **8**, 1325-1347.

Ciach, G. J., Morrissey, M. L. & Krajewski, W. F. (2000) Conditional bias in radar rainfall estimation. *J. Appl. Met.* **39**, 1941–1946.

Downer, C. W. & Ogden, F. L. (2002) GSSHA *User's Manual, Gridded Surface Subsurface Hydrologic Analysis Version 1.43 for WMS 6.1*. Engineer Research and Development Center Technical Report, Vicksburg, USA.

Downer, C. W. & Ogden, F. L. (2004) Prediction of runoff and soil moisture at the watershed scale: effects of model complexity and parameter assignment. *Water Resour. Res.* **39**(3), doi:10.1029/2002WR001439.

Fulton, R. A., Breidenbach, J. P., Seo, D.-J., Miller, D. A. & O'Bannon, T. (1998) The WSR-88D rainfall algorithm. *Weather and Forecasting* **13**, 377–395.

Germann, U., Berenguer, M., Sempere-Torres, D. & Salvade, G. (2006) Ensemble radar precipitation estimation -a new topic on the radar horizon. In: *Proc. ERAD Fourth European Conference on Radar in Meteorology and Hydrology* (Barcelona, Spain, 18-22 September 2006, 559-562). **[details please]**

Gourleya, J. J. & Vieux, B. E. (2006) A method for identifying sources of model uncertainty in rainfall–runoff simulations. *J. Hydrol.* **327**(1-2), 68–80.

Habib, E. & Krajewski, W. F. (2001) Estimation of rainfall interstation correlation. *J. Hydromet.* **2**, 621–629.

Habib, E., Krajewski, W. F. & Kruger. A. (2001) Sampling errors of tipping-bucket rain gauge measurements. *J. Hydrol. Engng ASCE* **13**, 159–166.

Habib, E., Ciach, G. J. & Krajewski, W. F. (2004) A method for filtering out raingauge representativeness errors from the verification distributions of radar and raingauge rainfall *Adv. Water Resour*. **27**(10), 967–980.

Hossain, F. & Anagnostou, E. N. (2006) A two dimensional satellite rainfall error model. *IEEE Trans. Geosci. Remote Sensing*. **44**, doi:10.1109/TGRS.2005.863866.

Hossain, F., Anagnostou, E. N., Borga, M. & Dinku, T. (2004) Hydrological model sensitivity to parameter and radar rainfall estimation uncertainty. *Hydrol. Processes* **18**(17), 3277–3299, doi:10.1002/hyp.5659.

Hunter, S. (1996) WSR-88D radar rainfall estimation: capabilities, limitations and potential improvements. *NWA Digest* **20**, 26–36.

Jayakrishnan, R., Srinivasan, R. & Arnold, J. G. (2004) Comparison of raingage and WSR-88D stage precipitation data over the Texas–Gulf basin. *J. Hydrol.* **292**, 135–152.

Johnson, D., Smith, M., Koren, V. and & Finnerty, B. (1999) Comparing mean areal precipitation estimates from NEXRAD and rain gauge networks. *J. Hydrol. Engng ASCE* **4**(2), 117–124.

Jordan P. W., Seed, A. W. & Weinmann, P. E. (2003) A stochastic model of radar measurement errors in rainfall accumulations at catchment scale. *J. Appl. Met.* **4**, 841–855.

Kessler, E. & Neas, B. (1994) On correlation, with applications to the radar and raingage measurement of rainfall. *Atmos. Res.* **34**, 217–229.

Krajewski, W. F. & Georgakakos, K. P. (1985) Synthesis of radar-rainfall data. *Water Resour. Res.* **21**, 764–768.

Krajewski, W. F. & Smith, J. A. (2002) Radar hydrology: rainfall estimation. *J. Hydrol.* **25**, 1387–1394.

Krajewski, W. F., Raghavan, R. & Chandrasekar, V. (1993) Physically based simulation of radar rainfall data using a space–time rainfall model. *J. Appl. Met.* **32**, 268–283.

Morin, E., Maddox, R. A., Goodrich, D. & Sorooshian, S. (2005) Radar Z-R relationship for summer monsoon storms in Arizona. *Weather Forecast.* **20**(4), 672–679.

Neary V., Habib, E. & Fleming, M. (2004) Hydrologic modeling with NEXRAD precipitation. *J. Hydrol. Engng ASCE* **9**(5), 339–349.

Nijssen, B. & Lettenmaier, D. P. (2004) Effect of precipitation sampling error on simulated hydrological fluxes and states: anticipating the global precipitation measurement satellites. *J. Geophys. Res. – Atmos.* **109**, D02103, doi:10.1029/2003JD003497.

Obled, C., Wending, J. & Beven, K. (1994) The sensitivity of hydrological models to spatial rainfall patterns: an evaluation using observed data. *J. Hydrol.* **159**, 305–333.

Ogden, F. L. & Julien, P. Y. (1993) Runoff sensitivity to temporal and spatial rainfall variability at runoff plane and small basin scales. *Water Resour. Res.* **29**(8), 2589–2597.

Ogden, F. L. & Saghafian, B. (1997) Green and Ampt infiltration and redistribution. *J. Irrig. Drain. Engng* **123**, 386–393.

Pessoa, M. L., Bras, R. L. & Williams, E. R. (1993) Use of weather radar for flood forecasting in the Sieve river basin: a sensitivity analysis. *J. Appl. Met.* **32**, 462–475.

Rico-Ramirez, M. A., Cluckie, I. D., Shepherd, G. & Pallot, A. (2007) A high resolution radar experiment on the island of Jersey. *Meteorol. Applications* **14**, 117–129.

Reed, S. M. & Maidment, D. R. (1999) Coordinate transformations for using NEXRAD data in GIS-based hydrologic modeling. *J. Hydrol. Engng ASCE* **4**(2), 174–182.

Senarath, S. U. S., Ogden, F. L., Downer, C. W. & Sharif, H. O. (2000) On the calibration and verification of distributed, physically-based, continuous, Hortonian hydrologic models. *Water Resour. Res.* **36**, 1495–1510.

Seo, D.-J. & Breidenbach, J. P. (2002) Real-time correction of spatially nonuniform bias in radar rainfall data using rain gauge measurements. *J. Hydromet.* **3**, 93–111.

Sevruk, B. & Lapin, M. (1993) Precipitation measurement and quality control. In: *Proc. Int. Symp. on Precipitation and Evaporation* (Bratislava), Vol 1. Slovak Hydrometeorological Institute and Swiss Federal Institute of Technology.

Sharif, H. O., Ogden, F. L., Krajewski, W. F. & Xue, M. (2002) Numerical simulations of radar rainfall error propagation. *Water Resour. Res.* **38**, 1140, doi:10.1029/2001WR000525.

Singh, V. P. & Woolhiser, D. A. (2002) Mathematical modeling of watershed hydrology, *J. Hydrol. Engng ASCE* **7**(4), 269–343.

Smith, J. A., Seo, D.-J., Baeck, M. L. & Hudlow, M. D. (1996) An intercomparison study of NEXRAD precipitation estimates. *Water Resour. Res.* **32**, 2035–2045.

Sun, S., Mein, R. G., Keenan, T. D. & Elliott, J. F. (2000) Flood estimation using radar and raingauge data. *J. Hydrol.* **239**, 4–18.

Tachikawa, Y., Vieux, B. E., Georgakakos, K. P. & Nakakita, E. (eds) (2003) *Weather Radar Information and Distributed Hydrological Modeling* (Proc. Symp., Sapporo Japan, 3–11 July 2003). IAHS Publ. 282. IAHS Press, Wallingford, UK.

Upton, G. J. G. & Rahimi, A. R. (2003) On-line detection of errors in tipping-bucket raingauges, *J. Hydrol.* **278**, 197–212.

Vieux, B. E. & Bedient, P. B. (1998) Estimation of rainfall for flood prediction from WRS-88D reflectivity: a case study, 17–18 October 1994. *Weather Forecast.* **13**(2), 407–415.

Vignal, B. & Krajewski, W. F. (2001) Large sample evaluation of two methods to correct range-dependent error for WSR-88D rainfall estimates. *J. Hydromet.* **2**(5), 490–504.

Wilson, J. W. & Brandes, E. A. (1979) Radar measurement of rainfall—a summary. *Bull. Am. Met. Soc.* **60**, 1048–1058.

Winchell, M., Gupta, H. V. & Sorooshian, S. (1998) On the simulation of infiltration- and saturation-excess runoff using radar-based rainfall estimates: effects of algorithm uncertainty and pixel aggregation. *Water Resour. Res.* **34**(10), 2655–2670.

Wood, S. J., Jones, D. A. & Moore, R. J. (2000) Accuracy of rainfall measurement for scales of hydrological interest, *Hydrol. Earth System Sci.* **4**(4), 531–543.

Young, C. B., Bradley, A., Krajewski, W. F., Kruger, A. & Morrissey, M. L. (2000) Evaluating NEXRAD multisensor precipitation estimates for operational hydrologic forecasting. *J. Hydromet.* **1**, 241–254.

Received 31 August 2006; accepted 22 February 2008